Balancing Cationic and Hydrophobic Content of PEGylated siRNA Polyplexes Enhances Endosome Escape, Stability, Blood Circulation Time, and Bioactivity *in Vivo*

Christopher E. Nelson,[‡] James R. Kintzing,[‡] Ann Hanna, Joshua M. Shannon, Mukesh K. Gupta, and Craig L. Duvall*

Department of Biomedical Engineering, Vanderbilt University, Nashville, Tennessee 37240, United States. [‡]C. E. Nelson and J. R. Kintzing contributed equally.

ABSTRACT A family of pH-responsive diblock polymers composed of poly[(ethylene glycol)-*b*-[(2-(dimethylamino)ethyl methacrylate)-*co*-(butyl methacrylate)], PEG-(DMAEMA-*co*-BMA), was reversible addition−fragmentation chain transfer (RAFT) synthesized with 0−75 mol % BMA in the second polymer block. The relative mole % of DMAEMA and BMA was varied in order to identify a polymer that can be used to formulate PEGylated, siRNA-loaded polyplex nanoparticles (NPs) with an optimized balance of cationic and hydrophobic content in the NP core based on siRNA packaging, cytocompatibility, blood circulation half-life, endosomal escape, and *in vivo* bioactivity. The polymer with 50:50 mol % of DMAEMA:BMA (polymer "50B") in the RAFT-polymerized block efficiently condensed siRNA into 100 nm NPs that displayed pH-dependent membrane disruptive behavior finely tuned for endosomal escape. *In vitro* delivery of siRNA with polymer 50B produced up to 94% protein-level knockdown of the model gene luciferase. The PEG corona of the NPs blocked nonspecific interactions with constituents of human whole blood, and the relative hydrophobicity of polymer 50B increased NP stability in the presence of human serum or the polyanion heparin. When injected intravenously, 50B NPs enhanced blood circulation half-life 3-fold relative to more standard PEG-DMAEMA (0B) NPs ($p < 0.05$), due to improved stability and a reduced rate of renal clearance. The 50B NPs enhanced siRNA biodistribution to the liver and other organs and significantly increased gene silencing in the liver, kidneys, and spleen relative to the benchmark polymer 0B ($p < 0.05$). These collective findings validate the functional significance of tuning the balance of cationic and hydrophobic content of polyplex NPs utilized for systemic siRNA delivery *in vivo*.

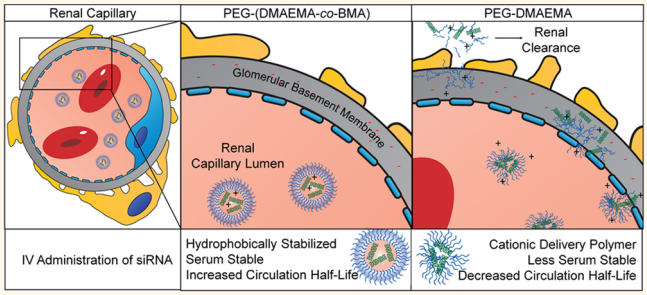

KEYWORDS: siRNA · reversible addition−fragmentation chain transfer (RAFT) polymerization · intravenous delivery · drug delivery · PEG · smart polymer · endosomal escape

Small interfering RNA (siRNA) is emerging as a therapeutic approach for potent, gene-specific silencing,[1] but clinical use of siRNA hinges on the development of safe and effective delivery technologies.[2] A variety of cationic biomaterials have been developed for siRNA packaging and delivery, including polymers, lipids, polysacaccharides, cell penetrating and fusogenic peptides, and dendrimers.[3,4] Cationic vehicles are effective for *in vitro* delivery because they condense siRNA into nanosized complexes with positive surface charge, which promotes endocytosis by electrostatically adsorbing onto anionic cell membranes.[5] However, intravenous administration of cationic lipoplexes or polyplexes, which is desirable for many therapeutic applications, often results in particle instability and nonspecific interactions with blood components that induce opsonization, aggregation of red blood cells, platelet activation, excessive biodistribution to the lungs, and, in extreme cases, rapid mortality.[6−9]

Polyethylene glycol (PEG) has been used extensively to improve the biocompatibility

* Address correspondence to craig.duvall@vanderbilt.edu.

Received for review June 29, 2013 and accepted September 16, 2013.

Published online September 16, 2013
10.1021/nn403325f

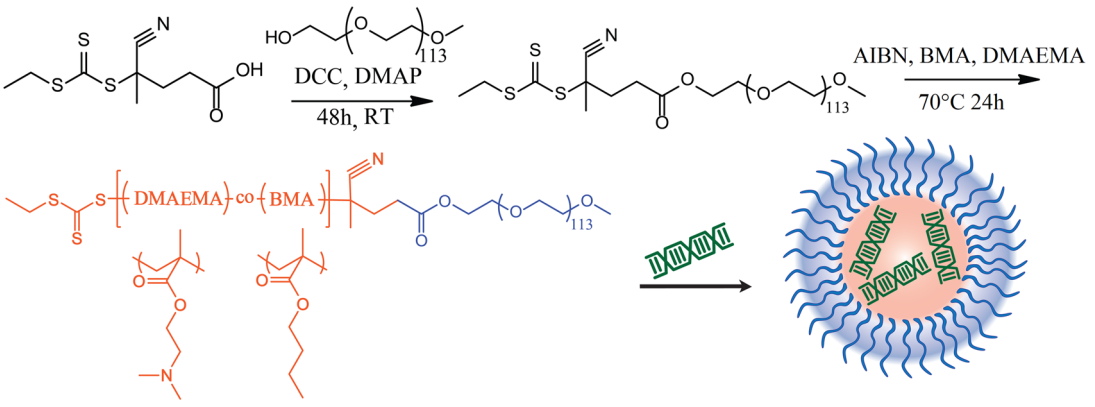

Figure 1. Polymer synthesis scheme for PEG-(DMAEMA-*co*-BMA).

of drug delivery nanoparticles and tissue engineered hydrogels. Functionalization of the exterior of drug delivery nanocarriers with PEG blocks adsorption of proteins, inhibits hemolysis or aggregation of erythrocytes, avoids immune stimulation, improves circulation time, protects the cargo from enzymatic degradation, and generally provides colloidal stability and "stealth".[10−15] PEGylation of cationic carriers has been successfully utilized to endow these properties to common polycations such as polyethyleneimine (PEI), poly-L-lysine, polyamidoamine (PAMAM), and poly(propyleneimine) (PPI) dendrimers, and poly(*N*,*N*-dimethylaminoethyl methacrylate) (PDMAEMA).[16−20]

Poly(EG-*b*-DMAEMA) (PEG-DMAEMA) demonstrates efficient siRNA packaging and relatively low cytotoxicity,[20] and studies on the effects of PEG architecture have shown that performance of a PEG-DMAEMA diblock structure is superior to brush or copolymer architectures.[12] PDMAEMA, like PEI, is believed to operate through the proton sponge effect for endosomal escape.[21,22] However, it has been found that active, pH-dependent membrane disruptive mechanisms improve intracellular bioactivity relative to pure proton sponge.[23] Recently, it has been shown that copolymerization of the hydrophobic monomer butyl methacrylate (BMA) with DEAMA or DMAEMA and propylacrylic acid (PAA) in a core-forming block[24,25] could be used to tune the pH-dependent membrane disruptive behavior of micelleplexes; these micelleplexes were designed to be preassembled, and nucleic acids were subsequently condensed onto coronas consisting of homopolymer blocks of DMAEMA.[26−28]

Hydrophobic modification has also been found to have other beneficial effects on cationic delivery systems including serum stability, membrane binding, improved dissociation in the cytoplasm, and decreased cytotoxicity.[29] Recently, a self-assembled micelleplex made from the triblock polymer poly(EG-*b*-nBA-*b*-DMAEMA) that packaged siRNA in the corona was found to have improved gene silencing *in vitro* and had increased tumor uptake relative to PEG-DMAEMA-based polyplexes.[30] While polymer blocks of DMEAMA with nBA are beneficial for stability, they do not generate polymers with active, pH-dependent membrane disruption behavior, possibly reducing the gene silencing activity due to endosomal entrapment. The polymers are also preassembled and condense siRNA onto the positively charged micelle corona that contains a mixture of PDMAEMA and PEG. Although it was not reported, this also presumably resulted in micelleplexes with a positive zeta potential, which would hinder *in vivo* circulation time and performance.[31,32]

In this work, a novel series of copolymers of DMAEMA and BMA, ranging from 0 to 75 mol % BMA, were synthesized using a simple, one-pot reversible addition−fragmentation chain transfer (RAFT) polymerization reaction from a PEGylated macro-chain transfer agent (macro-CTA). This polymer series was designed for core complexation of siRNA into PEG-corona polyplex nanoparticles (NPs) whose assembly is electrostatically triggered upon simple mixing with siRNA in buffer of appropriate pH. This strategy enables formulation of surface charge neutral siRNA-loaded NPs core-stabilized by a combination of electrostatic and hydrophobic interactions. The balance of cationic and hydrophobic content in the poly(DMAEMA-*co*-BMA) NP core-forming block was carefully titrated in order to identify improved PEGylated polycation variants that are optimized for *in vivo* performance based on a combination of improved stability and inertness in the blood circulation and pH-dependent membrane disruptive behavior finely tuned for efficient endosomal escape and cytoplasmic delivery. The performance of polyplexes made from PEG-(DMAEMA-*co*-BMA) polymers with varied quantities of BMA was benchmarked against the standardized and previously optimized PEG-DMAEMA diblock architecture.[20]

RESULTS AND DISCUSSION

Polymer Synthesis and Characterization. A series of pH-responsive diblock copolymers were synthesized from a PEG_{5K} macro-CTA using RAFT polymerization (Figure 1). Six polymers were synthesized with varied copolymer ratios of DMAEMA and BMA in the second block ranging from 0 to 75% BMA by adjusting the

composition in the feed (Table 1). The synthesis was completed by the RAFT polymerization technique, which has numerous advantages including formation of monodisperse polymers[33,34] as obtained here (all $M_w/M_n \leq 1.1$). Additionally, the single-step polymerization was a facile and scalable synthesis that yielded easily purified polymers with composition and molecular weight that closely matched the targeted values. This polymer series was designed to overcome the challenges related to systemic intravenous administration of polyplex nanoparticles with highly cationic surfaces.[7−9] It was posited that polyplex NPs comprising a PEG shell and a poly(DMAEMA-*co*-BMA) core would produce optimal properties for navigating both systemic circulation and intracellular (*i.e.*, endosomal) delivery barriers following intravenous delivery.

TABLE 1. Molecular Weight and Percent Composition of the Polymer Library

polymer name (% BMA in feed)	M_n(g/mol)[a]	PDI[a]	% BMA[b]	% DMAEMA[b]
0B	17 035	1.092	0.0	100.0
25B	18 747	1.075	23.8	76.2
40B	20 765	1.117	39.6	60.4
50B	18 040	1.040	48.3	51.7
60B	19 938	1.081	58.6	41.4
75B	17 349	1.053	74.5	25.5

[a] Determined by GPC. [b] Determined by ^{1}H NMR.

Characterization of pH-Dependent Polymer Micelle Assembly and Disassembly in the Absence of siRNA. In order to identify optimal formulation conditions for efficient siRNA packaging, dynamic light scattering (DLS) was used to assess the pH-dependent micelle assembly/disassembly behavior of the polymers across a range of pHs, from 7.4 to 4.0. As expected, the relative acidity required to trigger polymer micelle disassembly was directly related to the % BMA content in the poly(DMAEMA-*co*-BMA) block. The 0B and 25B polymers did not spontaneously form micelles at any pH tested, while polymers with 50% or more BMA content formed micelles (~25 nm diameter, Figure 2) at pH 7.4, with the 40B polymer appearing to be in a transition state at this pH. The 40B, 50B, and 60B polymeric micelles dissociated as the pH was lowered, and the pH where this transition occurred was inversely proportional to the % BMA in the polymer (Figure 2C−E, Figure 2D inset transmission electron microscopy (TEM) images visually confirmed NP assembly for 50B at pH 7.4).

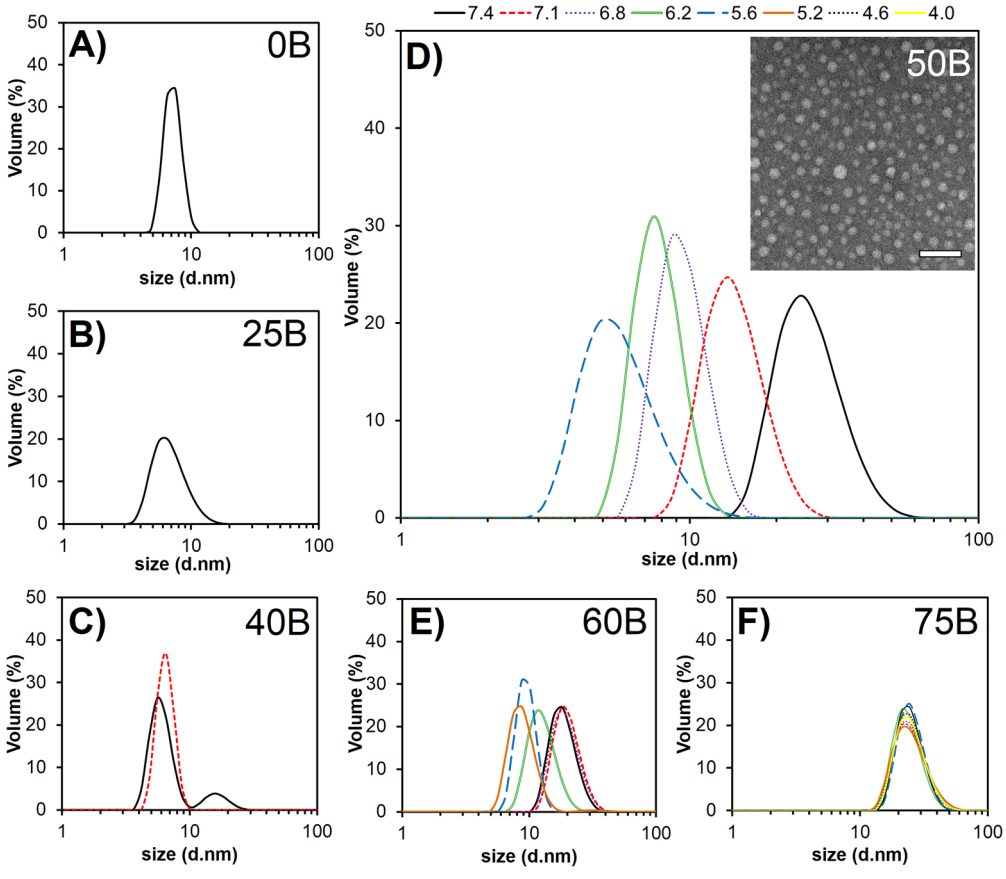

Figure 2. DLS measurements characterizing pH-dependent assembly/disassembly behavior of PEG-(DMAEMA-*co*-BMA)] polymers. DLS at varying pH values for polymers with (A) 0% BMA, (B) 25% BMA, (C) 40% BMA, (D) 50% BMA, (E) 60% BMA, and (F) 75% BMA. DLS data are shown for decreasing pH values down to pH 4.0 or until full NP disassembly occurred. Polymer 50B demonstrated the most dynamic pH-dependent behavior over the physiologically relevant range tested. The inset TEM of 50B polymer at pH 7.4 shows spherical nanoparticles (scale bar = 100 nm).

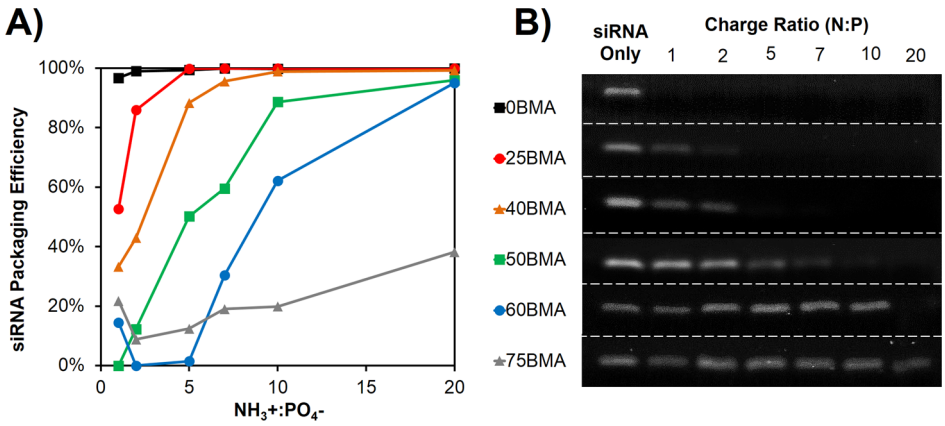

Figure 3. Formulation of siRNA polyplex NPs at pH 5.2. (A) siRNA packaging efficiency was dependent on both polymer composition and N:P ratio. (B) Gel images used to quantify siRNA packaging efficiency (concatenated image containing six gels, each of which was internally controlled for quantification purposes).

The 75B polymer remained in a stable micellar state at all pHs tested, suggesting that it did not accumulate sufficient cationic charge, even at pH 4.0, to destabilize the increased hydrophobic interactions between BMA (Figure 2F).

When the polymers are preassembled into micelles, the cationic poly(DMAEMA-*co*-BMA) polymer block is located in the particle core and is not readily accessible to electrostatically bind to siRNA. As a result, the polymers with a higher mole % of BMA in the poly(DMAEMA-*co*-BMA) block must be dissolved in a more acidic buffer to ensure that the DMAEMA tertiary amines are highly protonated, causing the polymers to exist as solubilized unimers due to electrostatic repulsion between poly(DMAEMA-*co*-BMA) blocks. In this unimeric state, the cationic polymer segments are fully exposed, and mixing with siRNA triggers electrostatic interactions that drive formation of polyplex NPs core-stabilized by electrostatic (PEG-DMAEMA) or a combination of electrostatic and hydrophobic interactions (PEG-(DMAEMA-co-BMA)). The data in Figure 2 suggest that polymers with 60 mol % BMA or less in the poly(DMAEMA-*co*-BMA) block exist in a unimeric state at pH 5.2, and as a result, this pH was used for formulation of siRNA-loaded polyplex NPs in subsequent studies.

Assembly and Characterization of siRNA-Loaded Polyplex NPs. The polymers were mixed with siRNA at pH 5.2 to trigger polyplex NP formation, and it was found that the N:P ratio required to fully complex siRNA was proportional to the % BMA in the polymer. Agarose gel electrophoretic mobility shifts were used to calculate the % siRNA packaging efficiency achieved using different formulation conditions (Figure 3). However, even polymers 40B and 50B were able to efficiently package siRNA at an N:P of 10 or greater. In contrast, the 75B polymers were found to encapsulate only 38% of the siRNA even at an N:P of 20. The polyplex NPs formed from all polymers at N:P of 10:1 had a hydrodynamic diameter of ~100 nm and approximately neutral zeta potential (Supplemental Figure S4). It was also found that reduction of the pH to 4.0 enabled efficient siRNA complexation of 50B at a lower charge ratio of 5:1, further supporting the importance of formation pH in siRNA packaging efficiency of these polymers (Supplemental Figure S5).

Cellular Uptake, Gene Silencing, and Cytotoxicity. Flow cytometry revealed that 0B polyplexes had the highest uptake and transfected nearly 100% of cells. 50B polyplex NPs were internalized significantly more than 40B or 60B (Figure 4A). Despite the higher relative uptake of 0B ($p < 0.05$), 50B polyplexes produced significantly greater luciferase silencing (94% reduction in the protein level at 48 h when compared to scrambled control siRNA) relative to all other polymers in MDA-MB-231 breast cancer cells transduced to constitutively express luciferase (Figure 4B, $p < 0.05$). Although the benchmark formulation (0B) produced the greatest uptake, it produced only 20% luciferase silencing. The increased gene silencing activity of 50B NPs suggests that they are more efficient in navigating intracellular delivery barriers (*i.e.*, increased cytoplasmic release) relative to 0B polyplexes. Treatment with the polyplex NPs was also shown to be nontoxic to MDA-MB-231 cells (not shown) and NIH3T3 fibroblasts at the concentrations used in gene silencing experiments (Figure 4C). The complete data set is listed in Supplemental Figures S8–S10.

Endolysosomal Escape. A major intracellular delivery barrier of siRNA nanocarriers is endosomal entrapment and trafficking for lysosomal degradation or exocytosis.[35] The current polymer family was designed to form polyplex NPs that destabilize at endolysosomal pHs, exposing the membrane disruptive poly(DMAEMA-*co*-BMA) polymer block. As a screen for active endosomal escape behavior, the pH-dependent membrane disruptive activity of siRNA-loaded polyplex NPs was measured using a red blood cell hemolysis assay.[36] At all N:P ratios tested, polyplexes made with 40B, 50B, and 60B generated switch-like, pH-dependent membrane disruption.

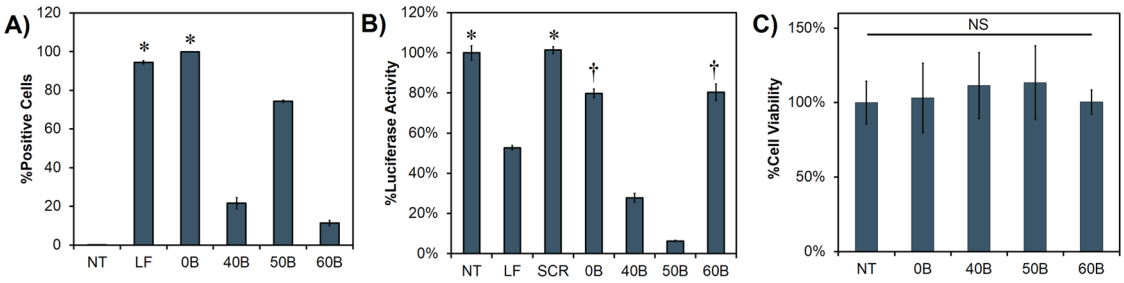

Figure 4. 50B-based polyplex NPs have the optimal combination of siRNA uptake, gene silencing bioactivity, and cytocompatibility *in vitro*. (A) Flow cytometry measurement of transfection efficiency and (B) bioluminescence measurement of luciferase knockdown *in vitro*; NT = no treatment, LF = Lipofectamine 2000, SCR = 50B polyplexes loaded with scrambled siRNA. (C) There was no cytotoxicity of any of the formulations at the concentrations tested. Statistical significance was evaluated by ANOVA at a confidence level of $p < 0.05$, and all groups were found to be significantly different except for the paired groups marked with *,†, or NS.

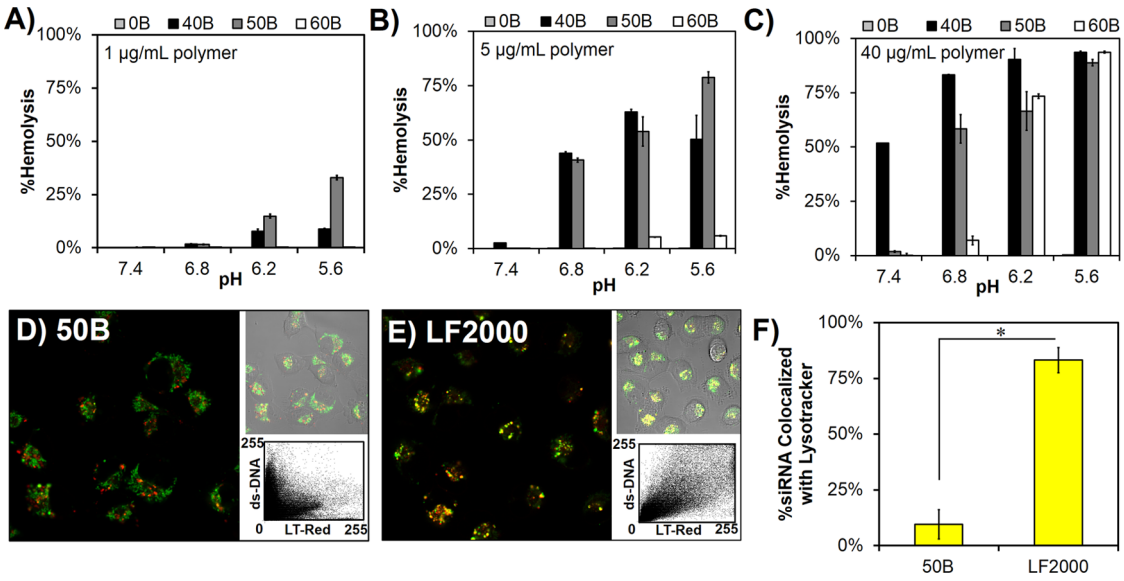

Figure 5. Polyplexes formulated with 50B show active endosome disruption and escape. (A–C) Hemolysis was both pH and composition dependent, with 50B siRNA polyplexes showing the most desirable pH-dependent membrane disruption behavior; 50B polyplexes did not disrupt erythrocyte membranes at pH 7.4, but produced robust hemolysis at pH 6.8, which is representative of early endosomes. All polyplexes were made at N:P of 10:1, and hemolysis was measured at (A) 1 μg/mL, (B) 5 μg/mL, and (C) 40 μg/mL polymer. (D, E) Confocal images showing colocalization of the endosome/lysosome dye Lysotracker with the cy5-labeled dsDNA cargo. Colocalization graphs are shown as insets. (F) 50B polyplexes showed decreased % colocalization of dsDNA cargo with lysosomes relative to Lipofectamine 2000 (* signifies $p < 0.01$).

Percent hemolysis of each polymer increased as the polymer concentration was increased and as the buffer pH was decreased. The pH where the hemolytic transition occurred mirrored the trend seen for destabilization of polymer NPs (Figure 2) and was inversely dependent on the % BMA content in the poly(DMAEMA-*co*-BMA) block (Figure 5A–C). Polyplex NPs made with the 50B polymer had optimal pH-responsive behavior based on producing membrane disruption in a pH environment representative of early and late endosomes but not at physiologic pH. Furthermore, the pH-dependent membrane disruptive behavior of 50B was similar between the polymer-only micelle and polyplex NP forms (Supplemental Figure S6). This suggests that the presence of the anionic siRNA did not inhibit pH-dependent particle destabilization and exposure of the membrane disruptive poly(BMA-*co*-DMAEMA) block of polyplex NPs exposed to acidic pH. Although they did not fully disassemble like the polymer-only micelles (Figure 2), the polyplex NP hydrodynamic diameter increased upon exposure to buffers of decreasing pH, suggesting that swelling and/or reorganization of the polyplex structure leads to exposure of the core-forming block under acidic conditions (Supplemental Figure S7).

To assess intracellular trafficking and endolysosomal escape, confocal microscopy was used to measure colocalization with the fluorescent dye Lysotracker. Diffuse staining of the cy5-labeled dsDNA cargo was visualized in cells incubated with 50B polyplexes for 24 h (Figure 5D), and 50B polyplex delivery resulted in significantly lower Lysotracker colocalization relative to Lipofectamine (colocalization appears yellow, Figure 5E). The colocalization was further visualized by

plotting color values of nonbackground image pixels in a dot plot where colocalized signal falls on the $y = x$ line, free siRNA falls on the *y*-axis, and lysosomes not containing siRNA fall on the *x*-axis (inset graphs). These combined data quantitatively and qualitatively suggest that polyplexes are able to efficiently overcome intracellular endolysosomal delivery barriers. This outcome is in agreement with the results from the pH-dependent hemolysis experiment, which suggests that 50B polyplexes are finely tuned to disrupt membranes in pH values representative of the endolysosomal pathway. These combined results suggest that 50B polyplexes improve the intracellular bioavailability of internalized siRNA, and this may mechanistically account for 50B having the highest gene silencing bioactivity of the polymers screened *in vitro* (Figure 4B).

Polyplex Stability and Hemocompatibility. For intravenous siRNA delivery systems, avoidance of destabilization and/or nonspecific interactions with cells and other blood components is key to general hemocompatibility and for maximizing blood circulation time in order to allow for passive tumor accumulation or active tissue targeting of intact, bioactive NPs. Nanoparticle PEGylation improves these properties,[37] and we hypothesized that optimization of the polyplex core could be an avenue to further enhance stability. Polyplex NPs made with 40B, 50B, and 60B were stable and did not aggregate or dissociate over a period of 24 h in phosphate-buffered saline (PBS) as assessed with DLS (Supplemental Figure S11). Förster resonance energy transfer (FRET) was used as another measure of stability, where 50B-NPs were co-loaded with FAM- and cy5-labeled dsDNA. FRET emission of the acceptor dye is observed only when the two fluorophores are co-encapsulated in the core of the NPs.[38] FRET-NPs made with 50B also retained an equivalent % FRET after 48 h of storage at room temperature, further indicating that siRNA remains stably encapsulated in the core of the polyplexes (Supplemental Figure S11).

Ex vivo experiments in human whole blood were done to measure nonspecific red blood cell interactions and stability of polyplexes. After a 1 h incubation in whole blood, polyplex NPs made with 50B were 74% retained in the serum fraction, whereas commercial standards PEI (5%) and Lipofectamine 2000 (48%) were more significantly associated with the cellular fraction following centrifugation (Figure 6A). As a measure of whole blood stability, FRET-NPs were incubated for 1 h in whole blood, and measurement of the FRET signal in the serum fraction showed that the 50B polyplex NPs retained a high % FRET signal of 77%, while Lipofectamine 2000 showed a significant ($p < 0.05$) decrease in relative % FRET to 35% of the baseline signal (Figure 6B).

Rapid urine excretion of many intravenously delivered cationic siRNA polyplexes occurs due to dissociation in the kidney glomerular basement membrane (GBM), which contains a high concentration of the anionic macromolecule heparan sulfate.[39,40] To model this phenomenon *in vitro*, we incubated FRET-NPs with heparinized saline (2 U/mL) and measured stability over time. This experiment showed that destabilization was dependent on the composition of the core-forming polymer block, indicating that 40−60% BMA resulted in significantly greater stability ($p < 0.05$) compared to 0B and 25B polyplex NPs (Figure 6C). Higher concentrations of heparin (>10 U/mL) were capable of dissociating the higher % BMA polyplexes 40B−60B (Supplemental Figure S12). These data suggest that incorporation of hydrophobic content into the core will slow the rate of kidney filtration of siRNA-loaded polyplex NPs.

Circulation Half-Life and Biodistribution. Increased resistance to heparin-mediated destabilization of 50B-based polyplex NPs was found to be functionally significant *in vivo* and yielded a 3.2-fold increase in the blood circulation half-life (18.4 ± 0.53 *vs* 5.80 ± 0.58 min) and 3.4-fold increase in area under the curve (AUC) (14.0 mg·h/L *vs* 4.1 mg·h/L) relative to the benchmark polymer 0B ($p < 0.05$ for both half-life and AUC, Figure 6D). The blood circulation half-life of 0B was consistent with previous studies on PEGylated polycationic siRNA carriers, which have typically shown values of <5 min and is associated with rapid decomplexation and systemic removal in the kidney.[39,40] Our combined data suggest that increased hydrophobicity in the core of polyplexes made with 50B polymers increased NP stability in the presence of heparin, slowed renal clearance *in vivo*, and increased blood circulation time. These data suggest 50B will biodistribute more efficiently to other tissues and will be potentially targeted more efficiently to tumors or other pathological sites.

To this end, tissue biodistribution of 0B and 50B siRNA polplex NPs was examined intravitally immediately following injection and at postmortem end points of 5 min, 20 min, 1 h, and 2 h postinjection. In agreement with the 50B polyplexes having less rapid renal decomplexation and siRNA removal through the urine acutely following injection, there was an immediate spike in concentration of siRNA in the kidneys of 0B polyplex-treated mice, and overall systemic clearance of siRNA delivered with 0B polyplex NPs was faster than following delivery with 50B polyplexes (Figure 6E,F). This trend is shown visually in representative mice (Figure 6G), and the full panel of intravital images is shown in Supplemental Figure S13. Imaging of kidneys excised from mice that were euthanized 5 min post-injection confirmed the intravital imaging data and showed a 2.2-fold increase in siRNA distribution in the kidney for 0B relative to 50B (Figure 6H). Liver biodistribution was noted at 5 min, 20 min, 1 h, and 2 h end points for 0B and 50B NPs and suggested that uptake in the liver is the primary route for removal of intact NPs (Figure 6I−K). There was a significantly greater quantity

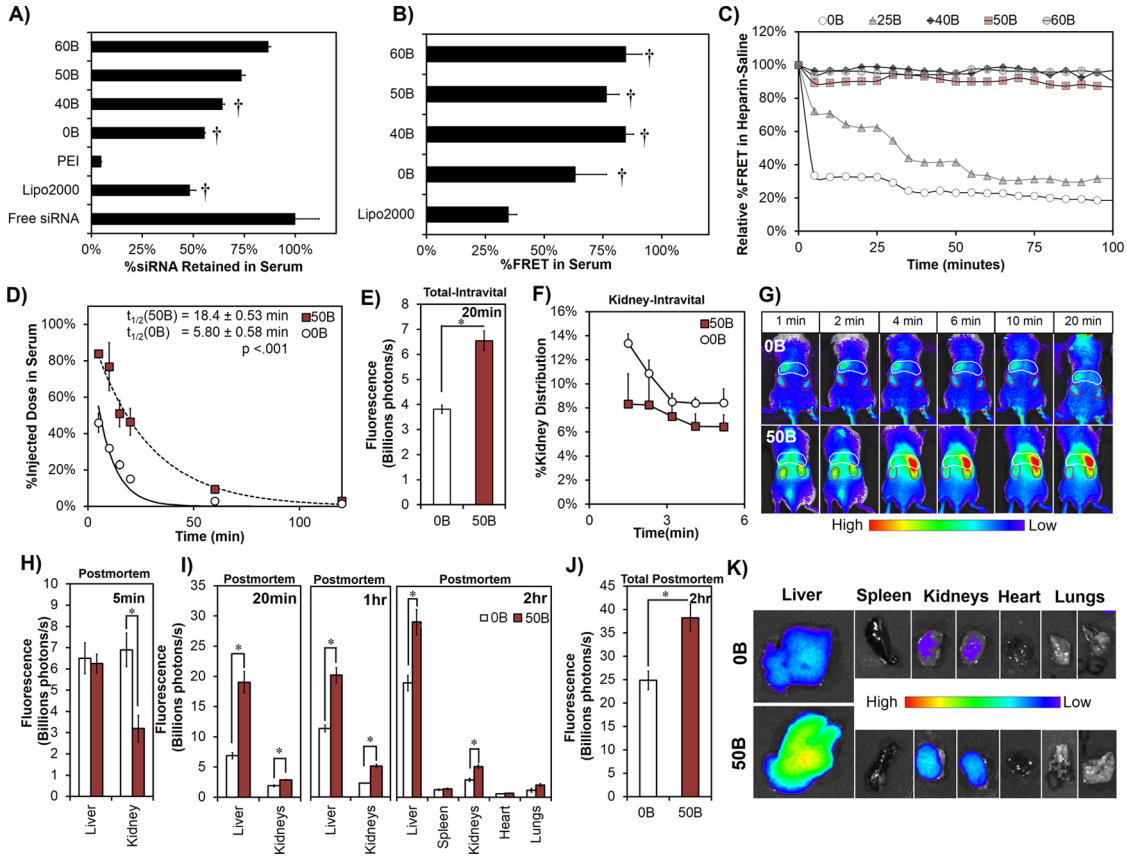

Figure 6. 50B polyplex NPs demonstrate enhanced stability upon exposure to heparin and human whole blood and have a longer circulation half-life and improved tissue biodistribution *in vivo*. (A) When incubated in blood at 37 °C, a significant fraction of the PEGylated polyplexes remained in the serum, indicating that they nonspecifically interact with erythrocytes to a significantly lesser degree than PEI ($p < 0.05$). (B) FRET-NP incubation in diluted human whole blood suggested that all PEGylated polyplex NPs were significantly more serum stable than the commercial standard Lipofectamine 2000 ($p < 0.05$). Statistical significance for A and B was evaluated by ANOVA at a confidence level of $p < 0.05$, where all groups were found to be significantly different except for those designated with †. (C) Stability of FRET-NPs incubated in 2 U/mL of heparin was enhanced for polyplexes with 40−60% BMA content in the core-forming polymer block. (D) The circulation half-life was 18.4 min for 50B and 5.8 min for 0B ($p < 0.05$, $n = 3$). (E) When measured intravitally, systemic biodistribution was significantly higher ($p < 0.05$) for the 50B-injected mice. (F) Intravital imaging of intravenously injected 50B and 0B polyplex NPs reveals rapid kidney distribution and systemic clearance of 0B. (G) Representative time course images are shown noting significantly more overall systemic biodistribution of fluorescent siRNA delivered *via* 50B polyplexes relative to the more rapidly cleared 0B polyplexes. (H) Imaging of siRNA fluorescence in kidneys excised at 5 min postinjection confirmed increased, rapid renal filtration of siRNA delivered *via* 0B polyplex NPs relative to the 50B group. (I) Postmortem tissue biodistribution showed preferential accumulation in liver and kidneys, with significantly decreased systemic clearance of 50B *vs* 0B at 20 min, 1 h, and 2 h postinjection ($p < 0.05$, $n = 3$). (J) Measurement of cumulative fluorescence in all of the organs at 2 h postinjection showed significantly increased biodistribution and retention in the organs for 50B relative to 0B polyplex NPs ($p < 0.05$). (K) Representative organ biodistribution images are shown from 2 h. Statistical significance for *in vivo* experiments was evaluated with ANOVA at a confidence level of $p < 0.05$, and * designates significant differences.

of siRNA in the liver and kidneys for 50B than 0B ($p < 0.05$) at 20 min, 1 h, and 2 h. Because 50B is partially susceptible to heparin decomplexation, the kidneys also have higher fluorescence at the later time points based on continued clearance of the longer-circulating 50B formulations. The integrated fluorescence across all organs was 1.5-fold higher in 50B polyplexes than 0B after 2 h ($p < 0.05$, Figure 6J), which is also consistent with slower removal through the urine and better overall biodistribution of 50B relative to 0B polyplexes. Importantly, we saw little uptake in the lungs and heart that would be associated with acute pulmonary toxicity that occurs with ineffectively shielded cationic polyplexes.[9]

The combined data from Figure 6 suggest that both polyplex surface PEGylation and incorporation of hydrophobic content in the core are beneficial for enhancing circulation half-life. PEG shielding improves circulation by decreasing aggregation with or adsorption to blood components, but does not fully shield the polyplex core from interaction with competing anions prevalent in the kidneys. The optimal combination of core hydrophobicity and PEG shielding achieved with 50B polyplexes increased the circulation half-life and is anticipated to improve passive tumor accumulation or, through functionalization with targeting ligands, retention in other target tissues. Poorer stability of 0B resulted in decreased systemic biodistribution due to

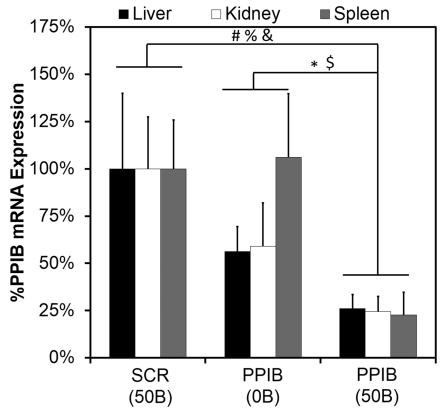

Figure 7. *In vivo* gene silencing following intravenous delivery of 50B polyplex NPs. Gene silencing of the model gene PPIB was evaluated by PCR 48 h after intravenous injection of 2 mg/kg siRNA doses. Significant differences were noted in the liver, kidney, and spleen between 50B and SCR groups ($p < 0.05$) and in the liver and spleen between 50B and 0B ($p < 0.05$). Markers of statistical differences: #,* liver; % kidney; &,$ spleen.

rapid decomplexation and removal through renal filtration. This agrees with previous literature suggesting that siRNA delivered *via* simple polycations is substantially excreted through the urine within 1 min postdelivery.[39,40]

PPIB Gene Silencing *in Vivo*. The last objective was to confirm that 50B polyplex NPs remained bioactive *in vivo*. The liver, kidneys, and spleen were selected as target tissues based on their known reticuloendothelial system (RES) function and the results of the biodistribution analysis. An siRNA targeting the model/housekeeping gene PPIB was delivered because of the consistent expression level of PPIB, and knockdown was analyzed in tissues extracted 48 h after intravenous injection. As shown in Figure 7, 50B polyplex NPs robustly silenced PPIB in the liver by ~74% following an intravenous dose of 2 mg/kg siRNA. Furthermore, 50B generated significantly greater gene silencing than 0B polyplexes injected at the same dose of 2 mg/kg ($p < 0.05$). Similarly, 50B polyplexes significantly silenced PPIB in the kidneys and spleen relative to scrambled controls ($p < 0.05$), and 50B silencing was significantly greater in the spleen relative to 0B ($p < 0.05$, for 0B *versus* 50B in the kidney). Improved *in vivo* gene silencing by 50B polyplexes relative to 0B is consistent with their active, pH-dependent membrane disruptive function and increased *in vitro* bioactivity, stability, circulation time, and overall tissue biodistribution. The similar level of gene silencing measured in the different organs also implies widespread tissue distribution of intact, bioactive 50B polyplex NPs and that these NPs may be used to preferentially accumulate in a variety of target tissues if implemented with the appropriate targeting ligand. Importantly, all polyplex injections were well tolerated by the mice, and no elevation in serum markers of liver toxicity ALT or AST were detected in mice treated with 50B or 0B at days 2 or 8 postinjection (Supplemental Figure S15).

CONCLUSIONS

We have synthesized and screened a small library of PEG-(DMAEMA-*co*-BMA) polymers for formulation of *in vivo*-ready siRNA nanocarriers designed to overcome key delivery barriers in the systemic circulation and inside target cells. PEG was used in the corona to impart hemocompatibilty and stability, and the combination of surface PEGylation and titration of hydrophobic content into the polyplex core resulted in better stabilized polyplexes with longer blood circulation times. The 50B polymer had optimally balanced cationic and hydrophobic content in the core-forming block and formed polyplex NPs with improved resistance against destabilization in the kidneys *in vivo* and pH-dependent membrane disruptive activity ideally tuned for endosomal escape. This resulted in slower renal clearance, increased circulation time, improved tissue biodistribution, and more potent gene silencing bioactivity *in vivo*. The 50B siRNA polyplex nanoparticles provide a promising platform for future applications involving enhanced permeability and retention (EPR)-driven delivery to tumors *in vivo* or active receptor–ligand targeting to increase accumulation and uptake in specific cells or tissues.

MATERIALS AND METHODS

Materials. All materials were obtained from Sigma-Aldrich and used as received unless otherwise noted. An alumna column was utilized to remove inhibitors from DMAEMA and BMA monomers, and final purification of polymers was done with PD10 desalting columns (GE Healthcare, Waukesha, WI, USA).

Synthesis of 4-Cyano-4-(ethylsulfanylthiocarbonyl)sulfanylpentanoic Acid (ECT) and PEG-ECT. The RAFT chain transfer agent ECT was synthesized as previously described,[24] and the R-group of the CTA was subsequently conjugated to PEG.[41] Briefly, dicyclohexylcarbodimide (4 mmol, 0.82 g) was added to the stirring solution of monomethoxy-poly(ethylene glycol) (M_n = 5000, 2 mmol, 10 g), ECT (4 mmol, 1.045 g), and DMAP (10 mg) in 50 mL of dichloromethane. The reaction mixture was stirred for 48 h. The precipitated cyclohexyl urea was removed by filtration, and the dichloromethanane layer was concentrated and precipitated into diethyl ether twice. The precipitated PEG-ECT was washed three times with diethyl ether and dried under vacuum (yield ~10g). ^{1}H NMR (400 MHz $CDCL_3$) revealed 91% substitution of the PEG (Supplemental Figure S1).

Polymer Synthesis and Characterization. RAFT polymerization was used to synthesize a library of copolymers using the PEG-ECT macro-CTA. In all cases, the degree of polymerization was 150, and the monomer plus CTA was 40% wt/v in dioxane. The polymerization reaction was carried out at 70 °C for 24 h using AIBN as the initiator with a 5:1 [CTA]:[Initiator] molar ratio. A series of polymerizations were carried out with monomer feed ratios of 0:100, 25:75, 40:60, 50:50, 60:40, and 75:25 mol % [BMA]:[DMAEMA]. The reaction was stopped by exposing the polymerization solution to air, and the resulting diblock polymers were precipitated into an excess of pentane. The isolated

polymers were vacuum-dried, redissolved in water, further purified using PD10 columns, and lyophilized. Polymers were characterized for composition and molecular weight by ^{1}H nuclear magnetic resonance spectroscopy (NMR, Bruker 400 MHz spectrometer equipped with a 9.4 T Oxford magnet). Absolute molecular weight of the polymers was determined using DMF mobile phase gel permeation chromatography (Agilent Technologies, Santa Clara, CA, USA) with inline Agilent refractive index and Wyatt miniDAWN TREOS light scattering detectors (Wyatt Technology Corp., Santa Barabara, CA, USA). All results are shown in Supplemental Figures S2 and S3.

Characterization of pH-Dependent Polymer Micelle Assembly and Disassembly in the Absence of siRNA. Each lyophilized polymer was dissolved in 100% ethanol, and aliquots of this solution were mixed with an 8-fold excess of phosphate buffer at pHs 7.4, 7.1, 6.8, 6.2, 5.6, and 5.2 or citrate buffers of 4.6 and 4.0 to make a 1 mg/mL stock solution. Each stock solution was diluted an additional 10-fold into phosphate or citrate buffer of the same pH to form 100 μg/mL polymer stocks, and the pH-dependence of self-assembly of each polymer into NPs was assessed using dynamic light scattering (Malvern Zetasizer Nano ZS, Malvern, UK). For imaging by transmission electron microscopy, carbon film-backed copper grids (Electron Microscopy Sciences, Hatfield, PA, USA) were inverted onto droplets containing aqueous NP suspensions (1 mg/mL) and blotted dry. Next, samples were inverted onto a droplet of 3% uranyl acetate, allowed to counterstain for 2 min, and again blotted dry. Finally, samples were desiccated *in vacuo* for 2 h prior to imaging on a Philips CM20 system operating at 200 kV (Philips, EO, The Netherlands).

Assembly and Characterization of siRNA-Loaded Polyplex NPs. Polyplex NPs loaded with siRNA were made by mixing pH 4.0 stock solutions of polymer and siRNA at N:P ratios of 5, 7, 10, or 20. The final charge ratio was calculated as the molar ratio of cationic amines on the DMAEMA (50% are assumed to be protonated at physiologic pH) to the anionic phosphates on the siRNA. After mixing, these solutions were diluted 5-fold to 100 μL with phosphate buffer to adjust the final pH to 7.4. After mixing, samples were incubated for 30 min, and 15 ng of siRNA for each sample was loaded onto a 4% agarose gel containing ethidium bromide to assess siRNA packaging efficiency. The gels were run at 100 V for 35 min and imaged with a UV transilluminator. Quantification was conducted using ImageJ version 1.45s (Freeware, NIH, Bethesda, MD, USA). Hydrodynamic diameter and zeta potential of the resulting polyplex NPs were measured using a Malvern Zetasizer Nano ZS.

Cell Culture. Human epithelial breast cancer cells (MDA-MB-231) were cultured in Dulbecco's modified Eagle's medium (DMEM, Gibco Cell Culture, Carlsbad, CA, USA) supplemented with 10% fetal bovine serum (FBS, Gibco) and 0.1% gentamicin (Gibco). Mouse embryonic fibroblasts (NIH3T3) were cultured in DMEM supplemented with 10% bovine calf serum (BCS, Gibco) and 1% penicillin−streptomycin (Gibco).

Flow Cytometry Assessment of siRNA Intracellular Delivery. MDA-MB-231 breast cancer cells were seeded in 24-well plates at a density of 40 000 cells/cm^2 and allowed to adhere overnight. The cells were treated with polyplexes loaded with Alexa488-labeled DNA (21mer duplexes mimicking siRNA molecules) at a final concentration in each well of 100 nM in media supplemented with 10% FBS. After the designated treatment time, cells were washed with PBS and trypsinized. Cells were centrifuged and resuspended in PBS containing trypan blue to quench extracellular fluorescence. Relative cell fluorescence was quantified *via* flow cytometry to measure NP intracellular delivery (FACSCalibur, BD Biosciences, Franklin Lakes, NJ, USA).

Cytotoxicity. Cytotoxicity of siRNA-loaded polyplex NPs was determined by measuring relative cell number based on luciferase activity. NIH3T3s were transduced with a lentivirus to constitutively express luciferase (LR-3T3s), and it was confirmed that cell number was directly proportional to luciferase signal (supplemental methods).[42] LR-3T3s were seeded in black-walled 96-well plates at a density of 12 500 cells/cm^2 and allowed to adhere overnight. Next, cells were treated with fresh polyplexes at concentrations of 50, 100, and 200 nM siRNA/well (100 μL volume, n = 5 for each treatment). After incubation for 24 h, the cells were given fresh luciferin-containing media (150 μg/mL). Bioluminescence was quantified using an IVIS Imaging System 200 series (Xenogen).

***In Vitro* Gene Silencing.** MDA-MB-231 breast cancer cells were transduced with a lentivirus to constitutively express luciferase (L231, supplemental methods). L231 cells were seeded in black, clear-bottom 96-well plates at a density of 12 500 cells/cm^2 and allowed to adhere overnight. Next, cells were treated for 24 h with polyplex NPs containing antiluciferase siRNA (Ambion) in 10% FBS media. Media was then replaced with luciferin-containing media (150 μg/mL), and bioluminescence was measured using an IVIS 200 Series imaging system (Xenogen). Next, cells were incubated for an additional 24 h in slow growth media (DMEM supplemented with 1% FBS, and 0.1% gentamicin), and bioluminescence was subsequently remeasured. Bioluminescence data were normalized to total protein content in cell lysates, which was measured *via* the Bradford assay (Bio-Rad).

Hemolysis Assay. Whole blood was extracted from anonymous, consenting human donors, and red blood cells (RBCs) were isolated according to well-established protocols.[36] RBCs were then incubated with the free polymers or with siRNA-loaded polyplex NPs (concentrations of 1−40 μg/mL) in buffers of pH 7.4, 6.8, 6.2, and 5.6, which model the environments in the extracellular space and in the more acidic vesicles of the endolysosomal pathway. After 1 h of incubation, the RBCs were centrifuged and the supernatant was spectrophotometrically analyzed at 451 nm in order to determine percent hemolysis relative to Triton X-100 detergent.

Confocal Microscopy Imaging of Endolysosomal Escape. MDA-MB-231 cells were seeded at a density of 12 500 cells/cm^2 in eight-well chamber slides (Nunc, Thermo Fisher Scientific Inc., Waltham, MA, USA). The cells were treated with cy5-labeled dsDNA loaded polyplex NPs at 100 nM or Lipofectamine 2000 according to the manufacturer's specifications. After treatment, media was replaced with Lysotracker (Invitrogen Life Technologies, Grand Island, NY, USA) containing media (75 nM), and cells were incubated for 1 h before imaging with confocal microscopy (Zeiss LSM 710Meta, Oberkochen, Germany) equipped with differential interference contrast. Images were analyzed using ImageJ with a colocalization extension, JaCOP, previously described.[43]

Analysis of Polyplex Stability and Hemocompatibility. NPs were loaded with Förster resonance energy transfer (using FAM and Cy5) pair-labeled 23mer dsDNAs (a model for siRNA) (FRET-NPs). Fluorescent intensity was measured using a spectrophotofluorometer with an excitation wavelength of 488 nm (Jobin Yvon/Horiba Fluorolog-3 FL3-111, Horiba Scientific, Kyoto Japan). FAM emission was collected at 520 ± 3 nm, and Cy5 emission was obtained at 670 ± 3 nm. % FRET was calculated as a ratio of the fluorescent intensity as follows:

$$\%\ \text{FRET} = \frac{I_{670}}{I_{520} + I_{670}} \quad (1)$$

For serum stability measurements, FRET-NPs were added into human whole blood diluted 1:3 in PBS at 100 nM (50 nM for each DNA). Treated blood samples were loaded into a black, round-bottom 96-well plate and placed on a shaker for 5 min before incubating at 37 °C for 1 h. Plates were then centrifuged at 500*g* for 5 min, and then 50 μL of supernatant (diluted blood serum) from each well was transferred into a black, clear-bottom 96-well plate. Fluorescence was measured using a microplate reader, and % FRET was calculated using eq 1. In parallel experiments to assess hemocompatibility *ex vivo*, polyplex NPs loaded with FAM-labeled dsDNA were used to quantify the percent of NPs in the supernatant, as a measure of inertness, or ability to reduce nonspecific adsorption to or aggregation with RBCs.

Because siRNA decomplexation by heparan sulfate-containing glomerular basement membrane in the kidney is a primary cause for rapid systemic clearance of polycation-siRNA nanoparticles,[39,40] the stability of FRET-NPs was measured in the presence of 2 U/mL of heparin sodium salt in DPBS. The fluorescence emission was measured over time using a microplate reader with an excitation wavelength of 488 nm

and an emission wavelength of 670 nm (Tecan Infinite F500, Männedorf, Switzerland).

Biodistribution. Balb/c mice (6−8 weeks of age) were injected intravenously into the tail vein with polyplex NPs containing a dsDNA (model for siRNA) labeled with 5′ IRDye 800CW (Integrated DNA Technologies, IDT). Blood samples were collected at 2, 5, 10, 15, and 20 min (maximum two blood collections per mouse). Separate cohorts of mice were euthanized for additional blood sample collection and organ harvesting for biodistribution analysis at 5 min, 20 min, 1 h, and 2 h postinjection. Blood was centrifuged at 500*g* for 5 min, and the supernatant was measured for fluorescence using a plate reader (Tecan) with 790 nm excitation and 810 nm emission. In addition, mice were monitored intravitally using an IVIS 200 for the first 20 min postinjection in order to measure the kinetics of biodistribution to the liver and kidneys. The backs of mice were shaved the day before injection and imaged with the dorsal side facing the camera to visualize and measure kidney and liver biodistribution. Regions of interest were drawn around the liver, kidneys, and the entire mouse to measure organ-specific and total fluorescence, respectively. An IVIS 200 was used to quantify the biodistribution in the explanted lungs, heart, liver, kidney, and spleen using Living Image 4.3 quantification software.

***In Vivo* PPIB Silencing.** Balb/c mice (6−8 weeks of age) were injected intravenously into the tail vein with polyplex NPs containing a dicer-substrate siRNA designed against cyclophilin B (PPIB, IDT) at a dose of 2 mg/kg. Mice were sacrificed at 48 h, and the RNA was extracted from organs with TRIZOL (Invitrogen, Carlsbad, CA, USA) and purified with RNEasy spin column (Qiagen, Venlo, The Netherlands). The expression of PPIB was evaluated by RT-PCR using the ΔΔCt method normalizing to GAPDH.

Statistical Methods. All measurements are presented as mean ± standard error of the mean. ANOVA was used to determine statistical significance, and $p < 0.05$ was considered significant.

Ethics Statement. The animal studies were conducted with adherence to the guidelines for the care and use of laboratory animals of the National Institutes of Health (NIH). All experiments with animals were approved by Vanderbilt University's Institutional Animal Care and Use Committee (IACUC). Human whole blood was collected from anonymous donors in accordance with an approved Institutional Review Board (IRB) protocol.

Conflict of Interest: The authors declare no competing financial interest.

Acknowledgment. This research was supported by NIH R21EB012750, an NSF sponsored REU program (NSF#1005023), and Vanderbilt University School of Engineering. Dynamic light scattering and TEM were conducted through the use of the core facilities of the Vanderbilt Institute of Nanoscale Sciences and Engineering (VINSE). Confocal imaging was performed in the VUMC Cell Imaging Shared Resource (supported by NIH Grants CA68485, DK20593, DK58404, HD15052, DK59637, and Ey008126).

Supporting Information Available: Supplementary figures and methods are included. This material is available free of charge *via* the Internet at http://pubs.acs.org.

REFERENCES AND NOTES

1. Fire, A.; Xu, S. Q.; Montgomery, M. K.; Kostas, S. A.; Driver, S. E.; Mello, C. C. Potent and Specific Genetic Interference by Double-Stranded RNA in Caenorhabditis elegans. *Nature* **1998**, *391*, 806–811.
2. White, P. J. Barriers to Successful Delivery of Short Interfering RNA after Systemic Administration. *Clin. Exp. Pharmacol. Physiol.* **2008**, *35*, 1371–1376.
3. Li, H. M.; Nelson, C. E.; Evans, B. C.; Duvall, C. L. Delivery of Intracellular-Acting Biologics in Pro-Apoptotic Therapies. *Curr. Pharm. Des.* **2011**, *17*, 293–319.
4. Rettig, G. R.; Behlke, M. A. Progress toward *in Vivo* Use of siRNAs-II. *Mol. Ther.* **2012**, *20*, 483–512.
5. Mislick, K. A.; Baldeschwieler, J. D. Evidence for the Role of Proteoglycans in Cation-Mediated Gene Transfer. *Proc. Natl. Acad. Sci. U.S.A.* **1996**, *93*, 12349–12354.
6. Alexis, F.; Pridgen, E.; Molnar, L. K.; Farokhzad, O. C. Factors Affecting the Clearance and Biodistribution of Polymeric Nanoparticles. *Mol. Pharm.* **2008**, *5*, 505–515.
7. Lv, H.; Zhang, S.; Wang, B.; Cui, S.; Yan, J. Toxicity of Cationic Lipids and Cationic Polymers in Gene Delivery. *J. Controlled Release* **2006**, *114*, 100–109.
8. Dash, P. R.; Read, M. L.; Barrett, L. B.; Wolfert, M. A.; Seymour, L. W. Factors Affecting Blood Clearance and *in Vivo* Distribution of Polyelectrolyte Complexes for Gene Delivery. *Gene Ther.* **1999**, *6*, 643–650.
9. Verbaan, F. J.; Oussoren, C.; van Dam, I. M.; Takakura, Y.; Hashida, M.; Crommelin, D. J.; Hennink, W. E.; Storm, G. The Fate of Poly(2-Dimethyl Amino Ethyl)Methacrylate-Based Polyplexes after Intravenous Administration. *Int. J. Pharm.* **2001**, *214*, 99–101.
10. Petersen, H.; Fechner, P. M.; Martin, A. L.; Kunath, K.; Stolnik, S.; Roberts, C. J.; Fischer, D.; Davies, M. C.; Kissel, T. Polyethylenimine-Graft-Poly(Ethylene Glycol) Copolymers: Influence of Copolymer Block Structure on DNA Complexation and Biological Activities as Gene Delivery System. *Bioconjugate Chem.* **2002**, *13*, 845–854.
11. Rungsardthong, U.; Deshpande, M.; Bailey, L.; Vamvakaki, M.; Armes, S. P.; Garnett, M. C.; Stolnik, S. Copolymers of Amine Methacrylate with Poly(Ethylene Glycol) as Vectors for Gene Therapy. *J. Controlled Release* **2001**, *73*, 359–380.
12. Venkataraman, S.; Ong, W. L.; Ong, Z. Y.; Joachim Loo, S. C.; Ee, P. L.; Yang, Y. Y. The Role of Peg Architecture and Molecular Weight in the Gene Transfection Performance of Pegylated Poly(Dimethylaminoethyl Methacrylate) Based Cationic Polymers. *Biomaterials* **2011**, *32*, 2369–2378.
13. Mishra, S.; Webster, P.; Davis, M. E. Pegylation Significantly Affects Cellular Uptake and Intracellular Trafficking of Non-Viral Gene Delivery Particles. *Eur. J. Cell Biol.* **2004**, *83*, 97–111.
14. Sato, A.; Choi, S. W.; Hirai, M.; Yamayoshi, A.; Moriyarna, R.; Yamano, T.; Takagi, M.; Kano, A.; Shimamoto, A.; Maruyama, A. Polymer Brush-Stabilized Polyplex for a siRNA Carrier with Long Circulatory Half-Life. *J. Controlled Release* **2007**, *122*, 209–216.
15. Verbaan, F. J.; Oussoren, C.; Snel, C. J.; Crommelin, D. J.; Hennink, W. E.; Storm, G. Steric Stabilization of Poly-(2-(Dimethylamino)Ethyl Methacrylate)-Based Polyplexes Mediates Prolonged Circulation and Tumor Targeting in Mice. *J. Gene Med.* **2004**, *6*, 64–75.
16. Glodde, M.; Sirsi, S. R.; Lutz, G. J. Physiochemical Properties of Low and High Molecular Weight Poly(Ethylene Glycol)-Grafted Poly(Ethylene Imine) Copolymers and Their Complexes with Oligonucleotides. *Biomacromolecules* **2006**, *7*, 347–356.
17. Itaka, K.; Yamauchi, K.; Harada, A.; Nakamura, K.; Kawaguchi, H.; Kataoka, K. Polyion Complex Micelles from Plasmid DNA and Poly(Ethylene Glycol)-Poly(L-Lysine) Block Copolymer as Serum-Tolerable Polyplex System: Physicochemical Properties of Micelles Relevant to Gene Transfection Efficiency. *Biomaterials* **2003**, *24*, 4495–4506.
18. Luo, D.; Haverstick, K.; Belcheva, N.; Han, E.; Saltzman, W. M. Poly(Ethylene Glycol)-Conjugated Pamam Dendrimer for Biocompatible, High-Efficiency DNA Delivery. *Macromolecules* **2002**, *35*, 3456–3462.
19. Taratula, O.; Garbuzenko, O. B.; Kirkpatrick, P.; Pandya, I.; Savla, R.; Pozharov, V. P.; He, H. X.; Minko, T. Surface-Engineered Targeted Ppi Dendrimer for Efficient Intracellular and Intratumoral siRNA Delivery. *J. Controlled Release* **2009**, *140*, 284–293.
20. Deshpande, M. C.; Garnett, M. C.; Vamvakaki, M.; Bailey, L.; Armes, S. P.; Stolnik, S. Influence of Polymer Architecture on the Structure of Complexes Formed by PEG-Tertiary Amine Methacrylate Copolymers and Phosphorothioate Oligonucleotide. *J. Controlled Release* **2002**, *81*, 185–199.
21. Behr, J. P. The Proton Sponge, a Means to Enter Cells Viruses Never Thought Of. *M S-Med. Sci.* **1996**, *12*, 56–58.

22. Behr, J. P. The Proton Sponge: A Trick to Enter Cells the Viruses Did Not Exploit. *Chimia* **1997**, *51*, 34–36.
23. Lee, H.; Jeong, J. H.; Park, T. G. A New Gene Delivery Formulation of Polyethylenimine/DNA Complexes Coated with PEG Conjugated Fusogenic Peptide. *J. Controlled Release* **2001**, *76*, 183–192.
24. Convertine, A. J.; Benoit, D. S. W.; Duvall, C. L.; Hoffman, A. S.; Stayton, P. S. Development of a Novel Endosomolytic Diblock Copolymer for siRNA Delivery. *J. Controlled Release* **2009**, *133*, 221–229.
25. Duvall, C. L.; Convertine, A. J.; Benoit, D. S.; Hoffman, A. S.; Stayton, P. S. Intracellular Delivery of a Proapoptotic Peptide *via* Conjugation to a RAFT Synthesized Endosomolytic Polymer. *Mol. Pharm.* **2010**, *7*, 468–476.
26. Convertine, A. J.; Diab, C.; Prieve, M.; Paschal, A.; Hoffman, A. S.; Johnson, P. H.; Stayton, P. S. pH-Responsive Polymeric Micelle Carriers for siRNA Drugs. *Biomacromolecules* **2010**, *11*, 2904–2911.
27. Manganiello, M. J.; Cheng, C.; Convertine, A. J.; Bryers, J. D.; Stayton, P. S. Diblock Copolymers with Tunable pH Transitions for Gene Delivery. *Biomaterials* **2012**, *33*, 2301–2309.
28. Cheng, C.; Convertine, A. J.; Stayton, P. S.; Bryers, J. D. Multifunctional Triblock Copolymers for Intracellular Messenger RNA Delivery. *Biomaterials* **2012**, *33*, 6868–6876.
29. Liu, Z.; Zhang, Z.; Zhou, C.; Jiao, Y. Hydrophobic Modifications of Cationic Polymers for Gene Delivery. *Prog. Polym. Sci.* **2010**, *35*, 1144–1162.
30. Gary, D. J.; Lee, H.; Sharma, R.; Lee, J. S.; Kim, Y.; Cui, Z. Y.; Jia, D.; Bowman, V. D.; Chipman, P. R.; Wan, L.; *et al*. Influence of Nano-Carrier Architecture on *in Vitro* siRNA Delivery Performance and *in Vivo* Biodistribution: Polyplexes vs Micelleplexes. *ACS Nano* **2011**, *5*, 3493–3505.
31. Xiao, K.; Li, Y.; Luo, J.; Lee, J. S.; Xiao, W.; Gonik, A. M.; Agarwal, R. G.; Lam, K. S. The Effect of Surface Charge on *in Vivo* Biodistribution of PEG-Oligocholic Acid Based Micellar Nanoparticles. *Biomaterials* **2011**, *32*, 3435–3446.
32. Arvizo, R. R.; Rana, S.; Miranda, O. R.; Bhattacharya, R.; Rotello, V. M.; Mukherjee, P. Mechanism of Anti-Angiogenic Property of Gold Nanoparticles: Role of Nanoparticle Size and Surface Charge. *Nanomed.-Nanotechnol.* **2011**, *7*, 580–587.
33. Moad, G.; Chiefari, J.; Chong, Y. K.; Ercole, F.; Krstina, J.; Jeffery, J.; Le, T. P. T.; Mayadunne, R. T. A.; Meijs, G. F.; Moad, C. L.; *et al*. Living Free-Radical Polymerization by Reversible Addition-Fragmentation Chain Transfer: The RAFT Process. *Macromolecules* **1998**, *31*, 5559–5562.
34. Boyer, C.; Bulmus, V.; Davis, T. P.; Ladmiral, V.; Liu, J.; Perrier, S. Bioapplications of RAFT Polymerization. *Chem. Rev.* **2009**, *109*, 5402–5436.
35. Medina-Kauwe, L. K.; Xie, J.; Hamm-Alvarez, S. Intracellular Trafficking of Nonviral Vectors. *Gene Ther.* **2005**, *12*, 1734–1751.
36. Evans, B. C.; Nelson, C. E.; Yu, S. S.; Beavers, K. R.; J., K. A.; Li, H.; Nelson, H. M.; Giorgio, T. D.; Duvall, C. L. *Ex Vivo* Red Blood Cell Hemolysis Assay for the Evaluation of pH-Responsive Endosomolytic Agents for Cytosolic Delivery of Biomacromolecular Drugs. *J. Vis. Exp.* **2013**, *73*, e50166.
37. Bartlett, D. W.; Davis, M. E. Physicochemical and Biological Characterization of Targeted, Nucleic Acid-Containing Nanoparticles. *Bioconjugate Chem.* **2007**, *18*, 456–468.
38. Gupta, M. K.; Meyer, T. A.; Nelson, C. E.; Duvall, C. L. Poly(Ps-b-Dma) Micelles for Reactive Oxygen Species Triggered Drug Release. *J. Controlled Release* **2012**, *162*, 591–598.
39. Zuckerman, J. E.; Choi, C. H. J.; Han, H.; Davis, M. E. Polycation-siRNA Nanoparticles Can Disassemble at the Kidney Glomerular Basement Membrane. *Proc. Natl. Acad. Sci. U.S.A.* **2012**, *109*, 3137–3142.
40. Naeye, B.; Deschout, H.; Caveliers, V.; Descamps, B.; Braeckmans, K.; Vanhove, C.; Demeester, J.; Lahoutte, T.; De Smedt, S. C.; Raemdonck, K. *In Vivo* Disassembly of Iv Administered siRNA Matrix Nanoparticles at the Renal Filtration Barrier. *Biomaterials* **2013**, *34*, 2350–2358.
41. Chong, Y. K.; Le, T. P. T.; Moad, G.; Rizzardo, E.; Thang, S. H. A More Versatile Route to Block Copolymers and Other Polymers of Complex Architecture by Living Radical Polymerization: The RAFT Process. *Macromolecules* **1999**, *32*, 2071–2074.
42. Joshi, R. V.; Nelson, C. E.; Poole, K. M.; Skala, M. C.; Duvall, C. L. Dual pH- and Temperature-Responsive Microparticles for Protein Delivery to Ischemic Tissues. *Acta Biomater.* **2013**, *9*, 6526–6534.
43. Bolte, S.; Cordelieres, F. P. A Guided Tour into Subcellular Colocalization Analysis in Light Microscopy. *J. Microsc. (Oxford, U. K.)* **2006**, *224*, 213–232.